Rotational and Vibrational Spectroscopy and Ideal Gas Heat Capacity of HFC 134a (CF_3CFH_2)

Li-Hong Xu,[†,‡] Anne M. Andrews,[†,§] Richard R. Cavanagh,[||] Gerald T. Fraser,[†] Karl K. Irikura,[⊥] and Frank J. Lovas[†]

Optical Technology Division, Surface and Microanalysis Science Division, and Physical and Chemical Properties Division, National Institute of Standards and Technology, Gaithersburg, Maryland 20899

Jens-Uwe Grabow and Wolfgang Stahl[#]

Institut für Physikalische Chemie, Christian-Albrechts-Universität, Olshausenstrasse 40-60, 24098 Kiel, Germany

Michael K. Crawford* and Robert J. Smalley

Central Research and Development, DuPont, Wilmington, Delaware 19880-0356

Received: December 10, 1996; In Final Form: January 24, 1997[⊗]

The hydrofluorocarbon HFC 134a (CF_3CFH_2) is the primary replacement for the chlorofluorocarbon CFC 12 (CF_2Cl_2) in numerous applications, including automobile air conditioning and home and commercial refrigeration. Here we describe a comprehensive spectroscopic study of this molecule. Precise microwave frequencies and molecular constants have been obtained for the vibrational ground state with a pulsed-molecular-beam Fourier-transform microwave spectrometer. New isotopic ground-state microwave measurements have also been made to improve the ground-state structural determination. Infrared and Raman spectra have been obtained, and all 18 vibrations have been observed and assigned. A high-resolution (3 MHz) microwave-sideband CO_2 laser and an electric-resonance optothermal spectrometer have been used to observe the molecular-beam infrared spectrum in the vicinity of the low-resolution gas-phase feature at 975 cm^{-1} assigned here and in some of the earlier studies as the ν_{15}, A″-symmetry, CH_2 rock. Two nearly equal-intensity *c*-type bands are observed under high resolution with origins at 974.35 and 974.87 cm^{-1}. The presence of two vibrational bands of A″ symmetry is attributed to strong anharmonic mixing of the ν_{15} vibration with a nearby combination vibration. On the basis of our low-resolution infrared measurements, we identify the perturbing state as the $3\nu_{18} + \nu_8$ combination level. Finally, the experimental results are used to calculate the vibrational contribution to the heat capacity and are compared with the results of earlier experimental and theoretical work, including our own electronic-structure calculations using an HF/6-31G* basis set.

Introduction

Because of their less deleterious effect on the ozone chemistry of the upper atmosphere, there has been much recent interest in the fluorinated hydrocarbons (HFCs) as replacements for the chloroflurocarbons (CFCs) widely used in many industrial and consumer applications. To assess the utility of the HFCs as substitutes for the CFCs, it is necessary to have available fundamental chemical and physical data to allow estimates to be made of their thermodynamic properties, atmospheric spectra, toxicity, flammability, etc. For instance, rotational and infrared spectroscopic measurements provide rotational constants and vibrational frequency data that can be used for the direct calculation of the atmospheric spectra and thermodynamic properties of the HFCs.[1] In addition, the spectroscopic measurements provide reliable calibration points for optimizing basis sets or force fields for *ab initio* electronic-structure or molecular-mechanics calculations of various molecular properties.

There has been a large number of studies of the vibrational spectroscopy of fluorinated ethanes reported during the past 50 years. The spectra of these molecules are of intrinsic interest since a number of subtle interactions are expected to be present and comparison of accurate measurements with the results of calculations provides a stringent test of our level of understanding of intramolecular phenomena such as anharmonic and Coriolis coupling. In particular, the presence in these molecules of hindered internal rotation offers an excellent opportunity to enhance our understanding of the interactions that determine the conformations of organic molecules. The presence of the low-frequency torsional vibrations, however, also greatly complicates the spectroscopic measurements by introducing a high density of vibrational hot bands in spectra measured at room temperature, and it is as a result of all these factors that there has been considerable disagreement concerning the determination and assignment of the vibrations in these molecules. HFC 134a (CF_3CFH_2) has not been an exception to this observation, and it was our intention to improve upon the accuracy of the previous assignments by undertaking the comprehensive study described below. In the present paper we report the high-resolution molecular-beam microwave spectrum and molecular structure, low-resolution infrared and Raman spectra, and high-

* Corresponding author.
† Optical Technology Division.
‡ Present address: Department of Physical Sciences, University of New Brunswick, Saint John, N.B. Canada E2L 4L5.
§ Present address: Science and Technology Division, Institute for Defense Analysis, 1801 N. Beauregard St., Alexandria, VA 22311.
|| Surface and Microanalysis Science Division.
⊥ Physical and Chemical Properties Division.
Present address: Institut für Physikalische Chemie der Rheinisch-Westfälischen Technischen Hochschule Aachen, Templergraben 59, D-52056 Aachen, Germany.
⊗ Abstract published in *Advance ACS Abstracts,* March 1, 1997.

S1089-5639(96)04038-8 CCC: $14.00

resolution 10 μm infrared spectrum of HFC 134a, perhaps the most important of the HFCs, which is presently replacing CFC 12 (CF_2Cl_2) in refrigeration and air conditioning systems.

The microwave measurements, made with a pulsed-molecular-beam Fourier-transform microwave spectrometer, extend to higher resolution and to the mono-^{13}C substituted isotopomers the Stark-modulation waveguide-cell results of Ogata and Miki[2] on the ground and first excited torsional levels of the normal isotopic species. At the approximately 2 kHz resolution of the Fourier-transform measurements, no evidence is observed for any torsional splittings arising from internal rotation about the C−C bond. This observation is consistent with the high barrier to internal rotation of 15.0(6) kJ/mol implied by the torsional vibrational spacings obtained from low-resolution Raman measurements[8] and our low-resolution infrared data.

The low-resolution infrared and Raman measurements, in combination with earlier results,[3−11] are used to develop reliable assignments for all 18 vibrations. We also report integrated infrared band intensities and use our vibrational frequencies to calculate the ideal gas heat capacity for HFC 134a. The normal-mode assignments have also been compared with the results of *ab initio* calculations undertaken previously[7,11−13] and in the present work.

In the high-resolution infrared study we have used an ∼3 MHz resolution tunable-microwave-sideband CO_2 laser and an electric-resonance optothermal spectrometer to investigate the infrared spectrum of the 975 cm^{-1} band of HFC 134a. This band has been previously attributed to the A″ ν_{15} normal mode[4,6−11] or to the A′ ν_6 normal mode.[5] Our observed rotational spectrum shows the band to be *c*-type, definitively establishing the symmetry of the normal mode as A″. In addition, we find that the 975 cm^{-1} normal mode is in nearly 1:1 anharmonic resonance with an essentially degenerate combination vibration, with an anharmonic matrix element of ∼0.26 cm^{-1}. A consequence of the resonance is that the low-resolution Q-branch is less pronounced than typically expected for *c*-type bands. The degradation of the Q-branch is most likely the origin of the previous assignment[5] of the spectrum to an A′ normal mode.

Experimental Section

Low-resolution (0.05 cm^{-1}) infrared data were obtained with a Bruker 113v Fourier-transform infrared spectrometer using a 4.2 K Si composite bolometer in the far-infrared and a 77 K HgCdTe detector in the mid-infrared. Various gas presssures, measured with a Leybold capacitance manometer, were used.

Raman data were measured using a SPEX triple spectrometer, the 5145 Å line of an Ar ion laser, and a laser power of approximately 1 W at the sample. The data were obtained using a 90° scattering geometry and gas pressures of 50−100 kPa. Polarized data were also obtained to aid with vibrational assignments.

The microwave measurements were made using Balle−Flygare-type[14] pulsed-nozzle Fourier-transform microwave spectrometers at NIST[15] and Kiel.[16] Measurements were made for the normal species, and for both mono-^{13}C-substituted isotopomers in natural abundance, using the arrangement of Grabow and Stahl[17] in which the molecular beam is directed down the cavity axis. This configuration provides an approximate factor of 10 gain in sensitivity and resolution over the initial cross-cavity arrangement of Balle and Flygare.[14]

The electric-resonance optothermal spectrometer and tunable microwave-sideband CO_2 laser source have been described previously.[18] The resolution of the spectrometer is approximately 3 MHz. Although the absolute uncertainty of the frequency measurements is only 2 MHz (1σ), limited by our knowledge of the Doppler shift arising from the nonorthogonal crossing of the molecular and laser beams, the relative precision of the frequency measurements is nearly an order of magnitude better, ∼0.25 MHz (1σ). The infrared assignments were aided by microwave-infrared double resonance and by comparision of the infrared combination differences with the precise combination differences calculated from the new microwave measurements.

TABLE 1: Observed Fourier Transform Microwave Transition Frequencies (in MHz) for HFC 134a and ^{13}C Isotopomers[a]

J'	K_a'	K_c'	J''	K_a''	K_c''	CF_3CH_2F	$^{13}CF_3CH_2F$	$^{13}CF_3{}^{13}CH_2F$
6	2	4	6	1	5	7346.429		
5	2	3	5	1	4	7448.167		
4	2	2	4	1	3	7537.529		
3	2	1	3	1	2	7612.019		
2	2	0	2	1	1	7669.641		
2	2	1	2	1	2	7788.520		
3	2	2	3	1	3	7848.394		
4	2	3	4	1	4	7928.411		
5	2	4	5	1	5	8028.690		
1	1	1	0	0	0	8115.043	8113.651	8056.041
6	2	5	6	1	6	8149.399		
7	2	6	7	1	7	8290.709		
8	2	7	8	1	8	8452.810		
2	0	2	1	1	1	8560.437	8549.864	8515.507
9	2	8	9	1	9	8635.855		
3	1	3	2	2	0	8826.950		
10	2	9	10	1	10	8840.026		
11	2	10	11	1	11	9065.441		
3	1	2	2	2	1	9046.252		
4	2	3	3	3	0	9352.282		
4	2	2	3	3	1	9359.190		
13	2	12	13	1	13	9580.355		
5	3	3	4	4	0	9760.987		
5	3	2	4	4	1	9761.079		
6	4	2	5	5	1	10166.464		
6	4	3	5	5	0	10166.464		
15	2	14	15	1	15	10180.694		
7	5	2	6	6	1	10571.592		
7	5	3	6	6	0	10571.592		
2	1	2	1	1	1	11077.495	11069.568	10998.976
2	0	2	1	0	1	11116.833	11108.850	11047.470
2	1	1	1	1	0	11157.057	11149.014	11097.348
9	3	6	9	2	7	12774.564		
8	3	5	8	2	6	12812.316		
7	3	4	7	2	5	12839.261		
6	3	3	6	2	4	12857.533		
5	3	2	5	2	3	12869.143		
4	3	1	4	2	2	12875.915		
3	3	0	3	2	1	12879.409		
3	3	1	3	2	2	12881.708		
4	3	2	4	2	3	12882.797		
5	3	3	5	2	4	12885.146		
6	3	4	6	2	5	12889.399		
7	3	5	7	2	6	12896.299		
8	3	6	8	2	7	12906.691		
2	1	2	1	0	1	13633.890	13628.551	13530.939
3	0	3	2	1	2	14157.007	14142.393	14085.933
4	1	4	3	2	1	14303.283		
4	1	3	3	2	2	14703.364		
5	2	4	4	3	1	14909.007		
5	2	3	4	3	2	14925.125		
3	1	3	2	1	2		16604.034	16497.993
3	0	3	2	0	2		16662.095	16569.399
3	2	2	2	2	1		16663.827	16572.138
3	2	1	2	2	0		16665.662	16574.975
3	1	2	2	1	1		16723.200	16645.546

[a] One standard deviation uncertainties on the transition frequencies are ∼2 kHz.

Results

Microwave Spectroscopy and Molecular Structure Analysis. The initial microwave measurements for the normal isotopic

TABLE 2: Spectroscopic Constants for HFC 134a[a]

	ground state			ν_{15} Fermi dyad	
	CF_3CH_2F	$^{13}CF_3CH_2F$	$CF_3{}^{13}CH_2F$	upper component	lower component
A/MHz	5355.618 17(51)	5356.1852(10)	5318.6104(15)	5347.640(35)	5347.756(33)
B/MHz	2799.220 85(31)	2797.196 88(55)	2786.645 58(56)	2791.564(35)	2793.546(33)
C/MHz	2759.432 94(31)	2757.466 15(49)	2737.452 12(47)	2754.874(21)	2755.179(17)
δ_J/kHz	0			0.71(24)	
δ_K/kHz	1.766(52)	*b*	*b*	1.08(48)	0.40(49)
Δ_J/kHz	0.5012(87)	*b*	*b*	1.53(47)	
Δ_{JK}/kHz	4.3132(55)	*b*	*b*	1.2(14)	2.7(15)
Δ_K/kHz	-3.396(15)	*b*	*b*	−2.28(97)	−3.81(10)
ν/cm^{-1}				974.874 136(21)	974.345 616(8)
ζ				0.006 096(49)	
σ/kHz	3.1	2.1	1.7		3.4 MHz

[a] Uncertainties are one standard deviation from the least-squares fit in units of the least significant digit given. [b] Fixed at the values for the normal species.

species were guided by the Stark-modulation waveguide results of Ogata and Miki.[2] Both *a*- and *b*-type transitions are observed, sampling *J* levels up to 15 and K_a levels up to 4 for the most abundant isotopomer. The observed transitions for the normal and two ^{13}C isotopomers are given in Table 1. No evidence was found for any internal-rotation splittings at the better than 5 kHz resolution of the experiments, as expected for a molecule with such a high barrier and large reduced mass for internal rotation.

The observed transitions were least-squares fit to the Watson asymmetric-rotor Hamiltonian[19] in the A-reduced I^r representation to determine the rotational and centrifugal distortion constants listed in Table 2. The small ^{13}C data sets do not allow as complete a centrifugal distortion analysis as is possible for the ^{12}C species. Indeed, the present ^{13}C data are only sensitive to the Δ_J and Δ_{JK} distortion constants, primarily due to the lack of any $K_a = 2 \leftarrow 1$ and higher K_a transitions. Alternatively, we have fit the ^{13}C data by constraining the distortion constants to the ^{12}C values to obtain rotational constants that are corrected for δ_K and Δ_K contributions. The differences in the rotational constants obtained by fitting the ^{13}C data to *A*, *B*, *C*, Δ_J, and Δ_{JK} and to *A*, *B*, and *C* with the distortion constants constrained to the ^{12}C values are small (∼4 kHz). An error of 4 kHz in the rotational constants contributes insignificant errors to the bond lengths and angles determined in the structural analysis. The standard deviations of the fits of 2−3 kHz are close to the expected experimental precision of ∼2 kHz. For $CF_3{}^{13}CH_2F$ the $1_{11}-0_{00}$ transition is weighted zero in the fit, since its inclusion in the fit increases the standard deviation by a factor of 3. The frequency of this transition ($1_{11}-0_{00}$) is poorly determined due to unresolved F nuclear spin−spin hyperfine structure, which makes it difficult to resolve the Doppler doublets and thus accurately measure the center of the line. This hyperfine broadening does not affect significantly the higher *J* transitions since the hyperfine contribution to the line widths decreases with *J*.

On the basis of a single isotopic form of HFC 134a, Ogata and Miki[2] derived a partial structure. With our additional ^{13}C isotopic data, it is possible to improve upon their structural analysis. Due to the presence of four F atoms, which cannot be isotopically substituted, a number of assumptions must be made concerning the bond lengths and angles. As a starting point, we have selected the CF_3 geometry from CF_3CH_3 and the CH_2F geometry from CH_3CH_2F. Both of these species have been studied by microwave spectroscopy (MW) and electron diffraction (ED) methods,[20−23] and a summary of the derived structural parameters pertinent to the CF_3CH_2F species is given in Table 3. The F and F″ atoms lie in the *a*,*b*-plane trans to one another, while the F′ and H pairs are located symmetrically about the *a*,*b*-plane. Since the bond lengths and angles from the MW and ED studies are in close agreement, we use the average values from these data sets to serve as initial values for the CF_3CH_2F analysis. Several fits were carried out varying r_{CC}, the CCF(F′) angle, the CCF″ angle, and either a tilt of the symmetric CF_3 group or fitting the CCF and CCF′ angles independently. The results of these fits are shown in Table 4. A fit with the CF_3 group symmetric about the C−C bond axis (i.e. no tilt) gave a standard deviation of 0.06 uÅ^2, while fits with a tilt of CF_3 or an asymmetric CF_3 had standard deviations 5−6 times smaller. The fitted C−C bond length is correlated with the CF and CF′ bond lengths, and the CCF angle, since $P_{cc} = 1/2(I_a + I_b - I_c) = mr^2_{FF'} + mr^2_{HH}$. Thus, the uncertainty shown is larger than expected from the standard deviation of the fit and results from varying the C−F bond lengths by ±0.003 Å. The C−C distance may be calculated by the Kraitchman substitution method,[24] yielding a value r_S(C−C) = 1.511(2) Å, which is the mean of the fit 1 and fit 2 values in Table 4. A third fit was carried out in which r_{CC} was fixed at the substitution value and is listed in Table 4 as fit 3. The C−C distance agrees quite well with the values reported for CH_3CH_2F, 1.512(2) Å[22] and 1.502(5) Å,[23] and it is intermediate between the two values reported for CF_3CH_3, namely, 1.530(5) Å[20] and 1.494(3) Å.[21]

TABLE 3: Geometry Parameters Assumed in Structure Fits; One Sigma Uncertainties Are Given in Parentheses

parameter	MW	ED	average
	From CF_3CH_3		
r_{CF}; $R_{CF'}$/Å	1.335(5)	1.340(2)	1.338
∠CCF(F′)/deg	111.0(3)	111.9(2)	111.5
reference	20	21	
	From CH_3CH_2F		
$r_{CF''}$/Å	1.387(3)	1.397(4)	1.392
∠CCF″/deg	109.5(4)	110.4(2)	110.0
r_{CH}/Å	1.094(1)	1.097(2)	1.095
∠CCH	112.2(1)	113.6	112.8
reference	22	23	

TABLE 4: Structural Parameters Determined for HFC 134a; One Sigma Uncertainties Are Given in Parentheses

parameter	fit 1	fit 2	fit 3 (fix r_{CC})
r_{cc}/Å	1.514(6)	1.505(4)	1.511
∠CCF/deg	109.8(2)	111.21(1)	109.73(2)
∠CCF′/deg	111.21(2)	111.21(1)	111.21(1)
∠CCF″/deg	108.4(6)	108.5(3)	108.62(1)
CF_3−C tilt	0	1.9(1)	0
σ/uÅ^2	0.019	0.011	0.018

On the basis of a single isotopic form of HFC 134a, Ogata and Miki[2] derived a partial structure. With our additional ^{13}C isotopic data, it is possible to improve upon their structural analysis. Due to the presence of four F atoms, which cannot be isotopically substituted, a number of assumptions must be made concerning the bond lengths and angles. As a starting point, we have selected the CF_3 geometry from CF_3CH_3 and the CH_2F geometry from CH_3CH_2F. Both of these species have been studied by microwave spectroscopy (MW) and electron diffraction (ED) methods,[20−23] and a summary of the derived structural parameters pertinent to the CF_3CH_2F species is given in Table 3. The F and F″ atoms lie in the *a*,*b*-plane trans to one another, while the F′ and H pairs are located symmetrically about the *a*,*b*-plane. Since the bond lengths and angles from the MW and ED studies are in close agreement, we use the average values from these data sets to serve as initial values for the CF_3CH_2F analysis. Several fits were carried out varying r_{CC}, the CCF(F′) angle, the CCF″ angle, and either a tilt of the symmetric CF_3 group or fitting the CCF and CCF′ angles independently. The results of these fits are shown in Table 4. A fit with the CF_3 group symmetric about the C−C bond axis (i.e. no tilt) gave a standard deviation of 0.06 uÅ^2, while fits with a tilt of CF_3 or an asymmetric CF_3 had standard deviations 5−6 times smaller. The fitted C−C bond length is correlated with the CF and CF′ bond lengths, and the CCF angle, since $P_{cc} = 1/2(I_a + I_b - I_c) = mr^2_{FF'} + mr^2_{HH}$. Thus, the uncertainty shown is larger than expected from the standard deviation of the fit and results from varying the C−F bond lengths by ±0.003 Å. The C−C distance may be calculated by the Kraitchman substitution method,[24] yielding a value r_S(C−C) = 1.511(2) Å, which is the mean of the fit 1 and fit 2 values in Table 4. A third fit was carried out in which r_{CC} was fixed at the substitution value and is listed in Table 4 as fit 3. The C−C distance agrees quite well with the values reported for CH_3CH_2F, 1.512(2) Å[22] and 1.502(5) Å,[23] and it is intermediate between the two values reported for CF_3CH_3, namely, 1.530(5) Å[20] and 1.494(3) Å.[21]

Low-Resolution Infrared and Raman Spectroscopy. In Figure 1 we show the low resolution infrared and Raman spectra of HFC 134a. In Table 5 we list vibrational band positions determined from the infrared and Raman data of Figure 1. HFC 134a has C_s point group symmetry with the only symmetry element being a plane of symmetry that includes the C−C axis.

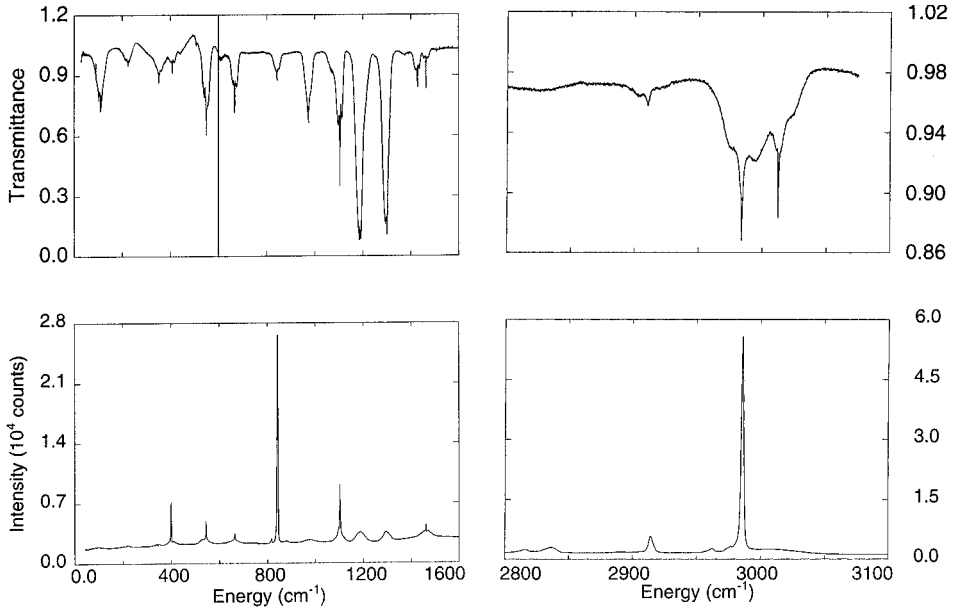

Figure 1. Infrared transmittance (top) and Raman (bottom) spectra of HFC 134a. The spectral resolution of the infrared spectrum is 0.2 cm^{-1}, while that of the Raman spectrum is about 1 cm^{-1}. The HFC 134a pressure was 101.3 kPa for the Raman data, whereas for the infrared spectrum pressures of 1.33 kPa were used in the far-infrared region (below 600 cm^{-1}) and 0.67 kPa in the mid- and near-infrared regions (above 600 cm^{-1}). The vertical line that appears at 600 cm^{-1} in the infrared spectrum separates the data measured at those two pressures. The path length of the gas cell used for the infrared measurements was 25.3 cm.

TABLE 5: Infrared and Raman Bands of HFC 134a (CF_3CFH_2); Band Positions Are Defined as Energies of Peak Intensities; Accuracies of Band Positions Are Estimated to be 1 cm^{-1} for the Infrared and 5 cm^{-1} for the Raman Measurements[a]

mode	symmetry	infrared (cm^{-1})	Raman (cm^{-1})	Raman polarization
ν_1	A′	2984	2985 vs	P
ν_2		1465	1464 m	P
ν_3		1429		P
ν_4		1298	1301 m	
ν_5		1186		
ν_6		1106	1107 m	P
ν_7		845	843 vs	P
ν_8		666	673 m	P
ν_9		549	557 m	P
ν_{10}		410	410 m	P
ν_{11}		226	230 vw	
ν_{12}	A″	3013	3010 w	DP
ν_{13}		1301	1301 m	DP
ν_{14}		1203	1189 m	DP
ν_{15}		975	975 w	DP
ν_{16}		533	542 w	
ν_{17}		351	355 w	
ν_{18}		109	113 vw	

[a] Point group: C_s. Irreducible representations: 11A′ + 7A″. Activity: infrared, 11A′ + 7A″; Raman, 11A′ + 7A″.

Group theory predicts that there should be a total of 18 vibrational modes, with 11 A′ (totally symmetric) and 7 A″ (non-totally symmetric) modes. Both A′ and A″ vibrations are infrared and Raman active. The Raman vibrations of A′ symmetry are expected to be (fully or partially) polarized, whereas the A″ vibrations are depolarized. The A′ vibrations, which have electric dipole transition moments parallel to the symmetry plane, will exhibit hybrid *a*/*b*-type infrared bands, whereas the A″ vibrations, which have transition dipole moments perpendicular to the symmetry plane, will exhibit *c*-type band shapes. Furthermore, since HFC 134a is a near-prolate asymmetric top ($\kappa = [(2B - A - C)/(A - C)] = -0.97$, where the rotational constants *A*, *B*, and *C* are given in Table 2), which is very close to being a symmetric top ($\kappa = -1$), it is expected that the A′ and A″ vibrational band shapes will appear, to first order, similar to the parallel and perpendicular bands of a symmetric top.[25] In Table 5 the polarizations are also listed for the more intense Raman lines. The total number of fundamentals observed and assigned is 18, consistent with the group theoretical prediction. The assignments given in Table 5 are generally consistent with the results of the earlier studies, although several differences will be discussed further below.

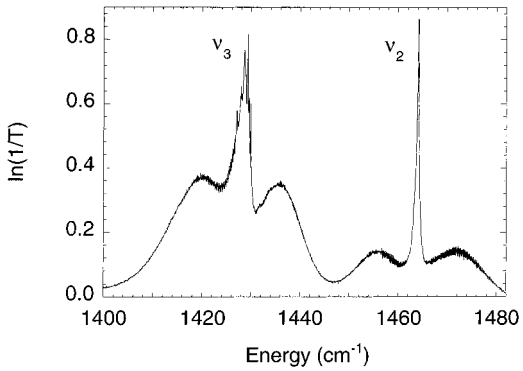

Figure 2. Infrared spectrum (0.05 cm^{-1} resolution) of HFC 134a showing the ν_2 and ν_3 modes.

In Table 6 we list the integrated infrared band intensities for HFC 134a. The integrated band intensities, *S*, are defined by[26]

$$S = \int_{\text{band}} a(\nu)\,\mathrm{d}\nu = \frac{1}{cd}\int_{\text{band}} \ln\left(\frac{I_0(\nu)}{I(\nu)}\right)\mathrm{d}\nu = \frac{1}{cd}\int_{\text{band}} \ln\left(\frac{1}{T(\nu)}\right)\mathrm{d}\nu$$

where $a(\nu)$ is the absorption intensity at frequency ν, $I_0(\nu)$ and $I(\nu)$ are the incident and transmitted intensities at frequency ν, respectively, $T(\nu)$ is the transmittance at frequency ν, *c* is the concentration, and *d* is the path length. The limits of integration for each band are also given in Table 6.

In Figure 2 we show details of the infrared spectrum between 1400 and 1500 cm^{-1}. The two bands shown are assigned as having A′ symmetry, with the ν_2 band at 1465 cm^{-1} exhibiting an *a*-type band shape, whereas the ν_3 band at 1429 cm^{-1} is of hybrid *a*/*b* nature. The symmetric appearance of ν_2 is indicative

TABLE 6: Integrated Infrared Line Strengths for HFC 134a in Units of km mol^{-1} [a]

	pressure (kPa)					
mode	0.067	0.67	0.69	1.33	3.33	Gauss94
ν_1 2955−3002	5.9	5.0			5.0	16.4
ν_2 1449−1494	5.9	5.6			4.3	9.0
ν_3 1398−1447	14.7	15.9			15.2	20.6
$\nu_4 + \nu_5$ 1148−1232	396.0	*sat*			*sat*	194.8
$\nu_5 + \nu_4$ 1148−1232		*sat*			*sat*	299.6
ν_6 1081−1128	72.1	*sat*			*sat*	111.8
ν_7 804−873	*weak*	18.5			17.3	19.7
ν_8 611−700	*weak*	40.4			*sat*	42.2
$\nu_9 + \nu_{16}$ 507−586	*weak*	13.8			10.8	13.3
ν_{10} 391−435			0.56	0.57	0.52	0.88
ν_{11} 180−262			2.3	2.7	2.6	4.1
ν_{12} 3002−3041	1.9	1.1			1.5	23.3
ν_{13} 1256−1329	294.4	*sat*			*sat*	199.3
ν_{14}						52.7
ν_{15} 930−1012	60.4	60.1				61.3
$\nu_{16} + \nu_9$ (see $\nu_9 + \nu_{16}$)						4.4
ν_{17} 324−387			1.6	1.6	1.2	1.3
ν_{18} 75−142			6.1	5.8	5.5	7.0

[a] Total pressure in each case was adjusted to 100 kPa using N_2. The gas cell path length was 25.3 cm. Spectral resolution was 0.05 cm^{-1}. Note that ($\nu_4 + \nu_5$) were not well enough resolved to be separately integrated, and ($\nu_1 + \nu_{12}$) were separately integrated, although they were only slightly better resolved. The peak integration limits (in cm^{-1}) are given beside each mode label in the first column. The accuracy of the intensity measurements is estimated to be ±20%. The notation *sat* means that the spectral line was saturated at that pressure.

of an unperturbed *a*-type band in which the ground- and excited-state rotational constants are approximately equal and similar to the constants of the related hot bands.[27]

In Figure 3 we show a section of the far-infrared spectrum (50−600 cm^{-1}) and the corresponding region of the Raman spectrum. There are two strong Q-branch Raman features that correspond with the A′ modes at 410 cm^{-1} (ν_{10}) and 549 cm^{-1} (ν_9) in the infrared spectrum. A third broad A′ symmetry Raman mode appears at 230 cm^{-1} (ν_{11}), while two modes of A″ symmetry appear at 355 cm^{-1} (ν_{17}) and 542 cm^{-1} (ν_{16}). The latter two modes have *c*-type infrared band shapes, whereas the mode at 230 cm^{-1} appears to have a *b*-type shape (that is, a central intensity minimum). It is interesting that the ν_{17} Raman mode at 355 cm^{-1} has a central minimum, similar to that of a *b*-type infrared band. However, since this is an A″ symmetry Raman mode, rather than having a dipole moment along the *b* principal axis (which would of course correspond to the case of an A′ symmetry infrared mode), here the central minimum implies that the α_{xz} component of the Raman polarizability tensor is nonzero for this vibration, leading to rotational transitions that have the same selection rules as for *b*-type infrared bands except for the additional presence of transitions in which $\Delta J = \pm 2$.[25] Thus the Raman band shape is consistent with the assignment of this vibration as having A″ symmetry. Similar consideration of the other infrared and Raman band shapes, combined with Raman polarization measurements, facilitated the assignments given in Table 5.

In Figure 4 we show detailed views of three infrared bands whose relation will be discussed further below in the section on high-resolution infrared spectroscopy of the 975 cm^{-1} vibrational band. Figure 4 shows the ν_{18} A″ torsion at 110 cm^{-1}, the ν_8 665 cm^{-1} A′ band assigned to a CF_3 symmetric deformation,[12] and the ν_{15} 975 cm^{-1} A″ band which has been assigned to the CH_2 rock.[12] The ν_{18} torsion is a *c*-type band that exhibits a considerable amount of sharp Q-branch structure, much of which presumably originates from hot bands, whereas the ν_8 band is an *a*/*b* hybrid. The ν_{15} band, which is discussed in detail below, is of *c*-type. In general the most reliable determination of vibrational assignments based upon band

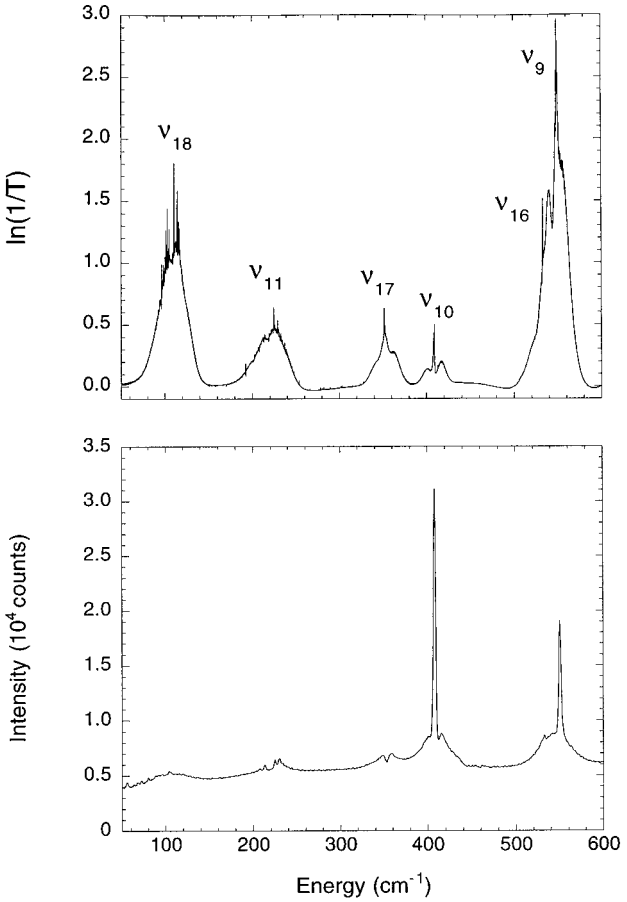

Figure 3. Far-infrared spectrum (0.05 cm^{-1} resolution) of HFC134a (top) and corresponding region of the Raman spectrum (bottom). The vibrations are labeled according to the assignments in Table 5.

shapes is made from the spectra of jet-cooled molecules, and such work can be found in ref 11.

High-Resolution Infrared Spectroscopy. The molecular-beam infrared spectrum of HFC 134a reveals that there are two *c*-type bands underneath the low-resolution gas-phase feature at 975 cm^{-1}. The two bands, with centers near 974.35 and 974.87 cm^{-1}, have nearly equal intensities, as can be seen in the sample spectra shown in Figure 5. Both bands originate from the vibrational ground state, as verified by microwave-infrared double resonance and precise ground-state combination differences. A total of 492 lines have been assigned for the lower frequency band, and a total of 480 lines have been assigned for the higher frequency band. Upper states are characterized with J values up to 28 and K_a values up to 7.

The observation that both bands have *c*-type electric-dipole selection rules establishes that the two upper state vibrations are both of A″ symmetry in C_s. This fact rules out the assignment of Nielsen and Halley,[5] who identified the low-resolution feature at 975 cm^{-1} with the *A*′ symmetry ν_6 normal mode. It is not likely that both of the observed vibrations are normal modes, however, since the harmonic force field generally does not allow two vibrations of the same symmetry to be effectively degenerate. We conclude, instead, that the two vibrations arise from a pair of interacting states. One of the two states is the normal-mode vibration that carriers the infrared intensity and the other state is a nearly degenerate vibration of the same symmetry that interacts anharmonically with the normal-mode vibration and borrows intensity through the interaction. The observation that the intensities for the two vibrations are nearly the same leads us to conclude that the two states are each nearly 1:1 mixtures of the normal-mode vibration and the background vibration. A pure 1:1 interaction implies

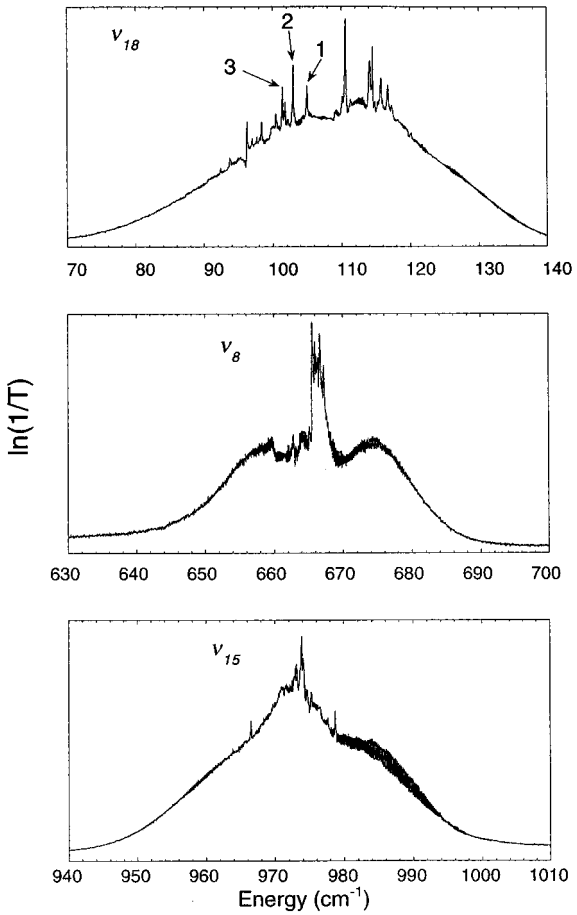

Figure 4. Infrared spectra (0.05 cm^{-1} resolution) of HFC 134a showing the ν_{18} torsion (top), the ν_8 CF_3 symmetric deformation (middle), and the ν_{15} CH_2 rock (bottom). The peaks labeled 1, 2, and 3 for the torsion (ν_{18}) are tentatively assigned as the $v = 1 \leftarrow 0$, the $v = 2 \leftarrow 1$, and the $v = 3 \leftarrow 2$ transitions. These assignments are described more fully in the text.

an anharmonic matrix element, *W*, of half the separation between the two observed vibrational band origins, i.e. $W \approx 0.26$ cm^{-1}.

Attempts were made to fit the rotational term values for the two bands to the Watson asymmetric-rotor Hamiltonian. The term values were determined by adding the calculated ground-state rotational energies to the observed infrared transition frequencies. This procedure does not contribute any significant error to the infrared analysis since the ground-state rotational term values are determined to a precision of ~100 times better than the infrared frequency measurements.

The term values for the lower frequency band are fit to a standard deviation of 8.2 MHz to a vibrational origin, ν_0, rotational constants, *A*, *B*, and *C*, and quartic centrifugal distortion constants, δ_J, δ_K, Δ_J, Δ_{JK}, and Δ_K (Table 2). The same set of constants fit the higher frequency vibration to a standard deviation of 12.9 MHz. These standard deviations are significantly larger than our typical measurement precision of ~0.25 MHz. For the higher frequency band the (observed−calculated) deviations are greatest for $K_a = 3$, and for the lower frequency band they are greatest for $K_a = 4$. These K_a values represent the closest approach of the K_a stacks for the two vibrations, for K_a values differing by 1. This observation suggests that the two anharmonically mixed vibrations are further coupled by a symmetry-allowed *c*-type Coriolis interaction which has matrix elements with $\Delta K_a = \pm 1$.

To determine the magnitude of the Coriolis interaction, we have fit the two vibrational states simultaneously to determine a set of rotational and centrifugal distortion constants for the two states, the band origins for the two states, and a Coriolis interaction constant, ζ, where the Coriolis operator is taken as $-2\zeta CJ_c$, were *C* is a rotational constant and J_c is the component of the angular momentum along the *c*-inertial axis. The constant $2\zeta C$ is actually determined in the fit; however, ζ is reported by dividing ζC by the final value for *C* of 2755 MHz. Also, the band origin for the lower state is fixed at the term value position of the 0_{00} state, so that only the difference between the band origins for the two states is determined. With the above fitting procedure, the rotational constants, distortion constants, and Coriolis constants are, in effect, determined in a representation in which the anharmonic and normal-mode part of the vibrational Hamiltonian are diagonal. To simplify the calculation of the Coriolis interaction, we quantize the body-fixed angular momentum along the *c*-inertial axis by using the III^r representation. Thus the centrifugal distortion constants obtained for the excited state cannot be directly compared with the ground-state values which were calculated in the I^r representation. The values of the ground-state distortion constants in the III^r representation are $\delta_J = 0.2294(38)$ kHz, $\delta_K = 1.7512(77)$ kHz, $\Delta_J = 0.960(16)$ kHz, $\Delta_{JK} = 2.938(23)$ kHz, and $\Delta_K = -3.397(15)$ kHz.

The results of the Coriolis fit are given in Table 2. The Coriolis constant determined from the fit is small, with $2C\zeta = 33.6(3)$ MHz. The rotational constants for the two states are nearly identical, consistent with our picture of nearly 1:1 mixing of the two zeroth-order vibrations by the anharmonic interaction. For the two vibrations the rotational constants differ by at most 0.07%, whereas they differ by as much as 0.3% from the ground-state values. Although the standard deviation of the fit is significantly better at 3.4 MHz, it is still more than a factor of 10 worse than the 0.25 MHz experimental precision. Ideally, to further improve the fit we would explicitly include the anharmonic interaction between the two states, since the model at its present level does not include *J* and K_a tuning of the unperturbed energy level separation over which the anharmonic matrix element operates through second-order perturbation theory. Unfortunately, this tuning of the resonance is extremely small, as evidenced by the small (3.4 MHz) standard deviation of the fit, and thus will not allow us to determine the anharmonic interaction strength precisely. We note, however, that both the relative intensities and the nearly identical rotational constants for the two states are consistent with an anharmonic matrix element of ~0.26 cm^{-1} between the two zeroth-order states.

***Ab Initio* Calculation of Vibrational Spectrum.** The vibrational spectrum of HFC 134a was calculated in the double-harmonic approximation at the Hartree−Fock level using the split-valence, polarized basis set 6-31G*.[28] Optimized molecular geometries and harmonic vibrational frequencies were calculated. As usual,[29] the calculated frequencies were scaled by 0.893 in order to predict fundamental vibrational frequencies, which are those observed experimentally.

In Table 7 we list the calculated structural parameters, vibrational frequencies, integrated infrared band intensities, Raman depolarization ratios, and rotational constants for HFC 134a. The calculated frequencies are compared with various experimental[3−7,10−12] and calculated[7,11,12] values from the literature in Table 8, while the calculated infrared band intensities are compared with the measured intensities in Table 6.

Calculation of Ideal Gas Heat Capacity. On the basis of our vibrational assignments, it is possible to calculate the vibrational heat capacity of HFC 134a, and in this section we describe that calculation. There has been a long history[31] of calculation of thermodynamic properties of gases from vibrational data, and such calculations have been reported for HFC 134a based upon measured vibrational energies[1,32] and calculated vibrational energies.[13] An equation of state that describes the

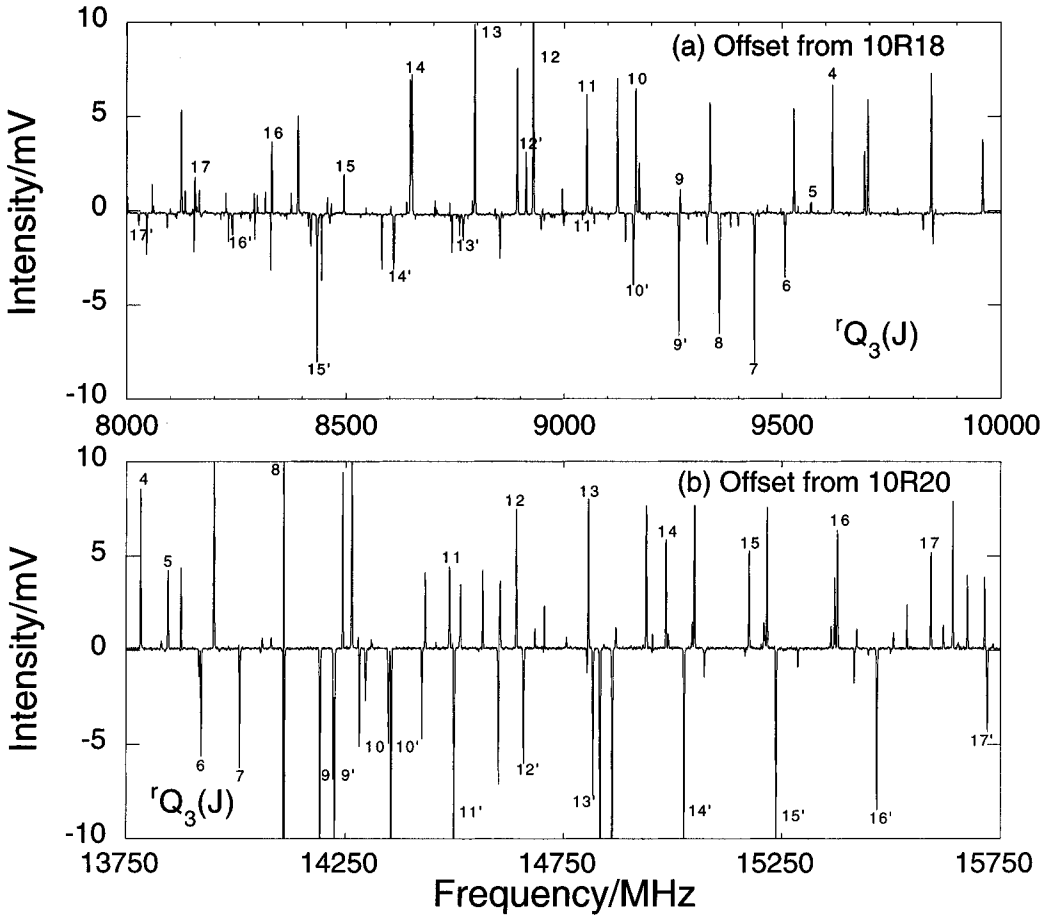

Figure 5. Portions of the high-resolution (2 MHz) infrared spectrum of jet-cooled HFC 134a showing the $^{r}Q_3$ Q-branches for the lower and upper component of the Fermi dyad. The numeric labels give the assignments. Two transitions for each J are shown due to assymetry doubling. The x-axis scale corresponds to the offset in MHz from either the R(18) or R(20) CO_2 laser lines at 974.621 940 cm^{-1} and 975.930 440 cm^{-1}, respectively.

thermodynamic properties of this refrigerant has also been developed recently.[33] The heat capacity of an ideal gas is given by

$$c_p^0 = c_p^{tr} + c_p^{rot} + c_p^{vib} \quad (1)$$

where tr, rot, and vib label the translational, rotational, and vibrational contributions. For a rigid nonlinear polyatomic molecule the translational and rotational contributions are given by

$$c_p^{tr} = \frac{5}{2}k_B N \quad (2)$$

and

$$c_p^{rot} = \frac{3}{2}k_B N \quad (3)$$

where k_B is Boltzmann's constant and N is Avogadro's number. In the harmonic oscillator approximation, the vibrational contribution to the heat capacity is given by

$$c_p^{vib} = NK_B \sum_{j=1}^{18} \frac{(\theta_j^{vib}/T)^2 e^{\theta_j^{vib}/T}}{(e^{\theta_j^{vib}/T} - 1)^2} \quad (4)$$

where the θ_j^{vib} are the vibrational frequencies in K, T is the absolute temperature, and the sum is over the 18 normal modes of vibration. Using these expressions we have calculated the heat capacity as a function of temperature, and the results are shown in Figure 6 (top). Also included for comparison in Figure 6 (top) is the heat capacity calculated using the scaled *ab initio* harmonic vibrational frequencies from Table 7.

In the specific heat calculation we have treated the hindered torsional vibration in several different ways for comparison. In Figure 6 (bottom) the torsional contribution to the heat capacity is shown assuming it to be a harmonic oscillator, a free rotor, and a hindered rotor with a rotational barrier height of ~15 kJ/mol ($V_3 = 1252$ cm^{-1} and $V_6 = 15$ cm^{-1}) and a moment of inertia $F = 1.1230$ cm^{-1}, as estimated by Lopata and Durig.[8] The assumption of an harmonic torsion is a reasonable approximation at low temperatures in light of the large barrier to internal rotation (15 kJ/mol ≈ 1800 K). On the other hand, as the temperature increases to values for which free internal rotation occurs, the contribution of this mode will become equal to $^1/_2 k_B N$.[25] Between the low- and high-temperature limits the torsional contribution to the heat capacity will be sensitive to the details of the true torsional potential energy function and will behave as shown in Figure 6 (bottom). It is interesting to note that near room temperature the torsion contributes nearly 10% of the ideal gas heat capacity. At high temperature the realistic treatment of the torsion slightly decreases the heat capacity compared with the harmonic approximation.

The calculated heat capacity is only weakly sensitive to small changes in the torsional barrier. For instance, if we change the torsional barrier from 15 kJ/mol to 14 kJ/mol, we find that the torsional contribution to the heat capacity changes by approximately 1%. The effect on the total heat capacity is an order of magnitude smaller at 0.1%. Our proposed torsional assignments discussed later suggest a barrier closer to 14 kJ/mol.

The most accurate treatment of the full heat capacity of HFC 134a is that based upon an equation of state (EOS),[33] which includes the effects of nonideality due to intermolecular

TABLE 7: Results of *ab Initio* Gaussian 94 Calculation; The Basis Set Was HF/6-31G*

Structural Parameters

parameter	value
r_{CC}	1.507 Å
r_{CF}	1.324 Å
$r_{CF'}$	1.318 Å
$r_{CF''}$	1.355 Å
r_{CH}	1.080 Å
∠CCF	109.1°
∠CCF′	111.7°
∠CCF″	108.7°
∠CCH	109.2°
dipole moment	2.14[a] D

Vibrational Energies, Integrated Infrared Band Intensities, Raman Band Intensities, and Raman Depolarization Ratios

mode	energy (cm^{-1})	infrared band intensity (km mol^{-1})	raman intensity (Å^4/amu)	raman depolarization ratio
A′				
ν_1	2929	16.4	88.9	0.10
ν_2	1482	9.0	7.32	0.748
ν_3	1445	20.6	0.769	0.48
ν_4	1301	194.8	1.85	0.70
ν_5	1214	299.6	2.37	0.748
ν_6	1100	111.8	4.05	0.50
ν_7	826	19.7	5.50	0.051
ν_8	644	42.2	1.46	0.72
ν_9	529	13.3	1.19	0.48
ν_{10}	397	0.88	1.16	0.51
ν_{11}	208	4.1	0.0346	0.43
A″				
ν_{12}	2984	23.3	47.4	0.75
ν_{13}	1312	199.3	4.73	0.75
ν_{14}	1198	52.7	5.46	0.75
ν_{15}	978	61.3	2.95	0.75
ν_{16}	515	4.4	0.591	0.75
ν_{17}	341	1.3	0.119	0.75
ν_{18}	104	7.0	0.0028	0.75

Rotational Constants (MHz)

A	*B*	*C*
5491.4	2866.4	2826.6

[a] Experimental values are 1.80 ± 0.22 D[2] and 2.058 ± 0.010 D.[30]

interactions. In that treatment[33] the ideal gas heat capacity was partly based upon speed of sound heat capacity measurements made over the temperature range 233−340 K and also upon caloric measurements of the real fluid to further extend the temperature range from 172 to 473 K. Vibrational data were excluded due to uncertainty arising from the torsional contribution to the heat capacity. We include in Figure 6 (top) a plot of the function used[33] to represent the ideal gas heat capacity in the EOS for HFC 134a. The heat capacities calculated using our vibrational data or the Gaussian 94 vibrational frequencies are in excellent agreement with the EOS results over the temperature range for which the EOS is stated to be accurate. Furthermore, our vibrational data extend the temperature range over which accurate experimental values of the ideal gas heat capacity are available. It is also worth noting that there has been a recent report of a calculation of the intermolecular interactions for several HFCs, including HFC 134a, utilizing molecular-dynamics simulations.[34] Thus one could in principle use the results of those calculations in combination with an *ab initio* calculation, such as Gaussian 94, to calculate real gas heat capacities, although perhaps not yet with the absolute precision required for applications.

Discussion

The results of a number of infrared and Raman studies summarized in Table 8 show a relatively consistent set of

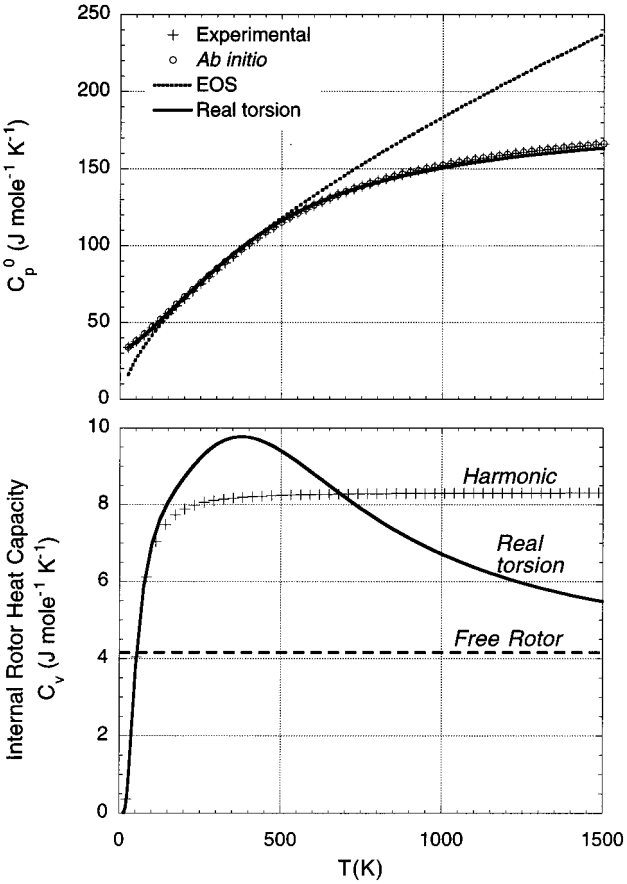

Figure 6. (top) Ideal gas heat capacity of HFC 134a, calculated using eqs 1−4 with the vibrational frequencies given in Table 5, including the rotational and translational contributions (crosses). The heat capacity calculated from the same vibrational data, but using a realistic torsional potential energy function with a barrier of ∼15 kJ/mol (V_3 = 1252 cm^{-1}, V_6 = 15 cm^{-1}) and F = 1.1230 cm^{-1} [8] in place of a harmonic torsion, is shown as a solid line. This yields a slight increase of the heat capacity just below 500 K and a decrease above 700 K. The result of the same calculation, using the vibrational frequencies predicted by the *ab initio* Gaussian 94 calculation (Table 7), is shown as open circles. Note that the *ab initio* result lies nearly on top of the experimental result. Finally, the ideal gas heat capacity used in an equation-of-state (EOS) treatment of the thermodynamic properties of HFC 134a[33] is shown as a dotted line. (bottom) The contribution of the internal rotation to the heat capacity for three different models, a harmonic oscillator, a free rotor, and a hindered rotor with a barrier of ∼15 kJ/mol (V_3 = 1252 cm^{-1}, V_6 = 15 cm^{-1}) and F = 1.1230 cm^{-1}.[8]

choices for the vibrational frequencies, particularly in the more recent studies. The experimental results are also fairly consistent with the results of the calculations presented in Table 7, and support the expectation that the *ab initio* techniques are accurate enough to make general vibrational band assignments for molecules as complex as these. Furthermore, the intensities predicted for the infrared bands (Table 6) are also quite close to those measured, although there are a few significant discrepancies. For example, the integrated intensities of the two highest frequency vibrations, the ν_1 and ν_{12} symmetric and asymmetric CH_2 stretches, are overestimated by nearly a factor of 10 in the calculation. The other calculated intensities are within a factor of 2 of the measured values, and in fact most are in considerably better agreement than that. It is possible that a higher level calculation using a larger basis set would give better results, although the problem could lie in the theory itself. For example, the double-harmonic approximation may not be valid for the large amplitude H vibrations which could exhibit accentuated anharmonic effects.

It is also worthwhile commenting upon the accuracy with which the *ab initio* calculation predicts the molecular structure

TABLE 8: Measured and Calculated Vibrational Energies (cm^{-1}) for HFC 134a, Including Normal Mode Assignments; Experimental Values Are on the Left Side of the Table (Bold Type), While Values Predicted by Theoretical Treatments Using the Basis Sets Listed Are Given on the Right (Plain Type)

mode	IR (this work and ref 10)	Raman (this work and ref 10)	IR (ref 11)	IR (ref 7)	IR (ref 4)	IR and Raman (ref 5)	IR and Raman (ref 1)	IR (ref 6)	HF/6-31G* (this work)	MP2/6-311 (ref 11)	MP2/6-31 (ref 7)	normal coordinate (ref 12)
A′												
ν_1	**2984**	**2985**	**2984**	**2981**	**2984**	**2984**	**2984**	**2986**	2929	3041	3169	2984
ν_2	**1465**	**1464**	**1464**	**1462**	**1431**	**1464**	**1464**	**1427**	1482	1476	1563	1431
ν_3	**1429**		**1430**	**1428**	**1296**	**1427**	**1427**	**1296**	1445	1447	1508	1371
ν_4	**1294**		**1294**	**1301**	**1096**	**1298**	**1298**	**1186**	1301	1304	1363	1298
ν_5	**1186**		**1186**	**1185**	**1067**	**1103**	**1103**	**1103**	1214	1191	1246	1191
ν_6	**1106**	**1107**	**1105**	**1104**	**908**	**972**	**972**	**1070**	1100	1109	1147	1096
ν_7	**845**	**843**	**844**	**843**	**844**	**843**	**842**	**846**	826	836	865	853
ν_8	**666**	**673**	**666**	**666**	**666**	**665**	**665**	**666**	644	655	668	661
ν_9	**549**	**557**	**549**	**549**	**550**	**549**	**549**	**557**	529	541	549	546
ν_{10}	**410**	**410**	**409**	**408**	**358**	**408**	**408**	**410**	397	406	413	385
ν_{11}	**226**	**230**	**225**	**225**	**201**	**225**	**225**	**222**	208	215	216	246
A″												
ν_{12}	**3013**	**3010**	**3013**	**3010**	**3015**	**3013**	**3013**	**3015**	2984	3112	3245	3015
ν_{13}	**1301**	**1301**	**1301**	**1294**	**1374**	**1182**	**1374**	**1463**	1312	1308	1360	1302
ν_{14}	**1203**	**1189**	**1203**	**1191**	**1189**	**665**	**1182**	**1296**	1198	1203	1247	1199
ν_{15}	**975**	**975**	**974**	**973**	**972**	**539**	**885**	**971**	978	971	1021	967
ν_{16}	**542**	**533**	**540**	**541**	**352**	**539**	**542**	515	524	530	545	
ν_{17}	**351**	**355**	**352**	**358**	**407**	**225**	**352**	**358**	341	348	358	358
ν_{18}	**109**	**113**	**109**	**110**	**124**	**120**	**120**	**112**	104	111	114	139

of HFC 134a. Comparing the results in Tables 2 and 4 (experiment) with those in Table 7 (calculation) leads us to the conclusion that the predictions of the *ab initio* calculation are in reasonably good agreement with the measured bond lengths and angles for HFC 134a. Other static molecular properties, such as the dipole moment, are also predicted fairly accurately. Thus it seems that calculations at the Hartree−Fock level, using a relatively small basis set such as HF/6-31G*, can serve as a reasonably accurate guide to the geometric, vibrational, and rotational properties of molecules as complex as HFC 134a, although for those that do not have 3-fold symmetric torsional potentials, such as HFC 134 (CF_2HCF_2H) and HFC 143 (CF_2-$HCFH_2$),[32] it would be desirable to make additional studies.

Turning now to a discussion of the high-resolution infrared spectroscopy of the 975 cm^{-1} band, in early infrared studies this band was assigned as both an A′ [5] and an A″ [4] symmetry fundamental. More recent work[6,7,10,11] supports the A″ assignment. Here we definitively establish the symmetry of the 975 cm^{-1} band as A″ from the observed rotational selection rules on the resolved rovibrational transitions. Furthermore, a recent study[11] of this band using high resolution Fourier-transform spectroscopy of HFC 134a molecules cooled in a molecular beam assigned the 975 cm^{-1} band to the ν_{15} fundamental interacting with the $\nu_{15} + \nu_{18} \leftarrow \nu_{18}$ hot band. To account for the observed intensity of this torsional hot band it was necessary to postulate that the torsion was not in thermal equilibrium with the other normal modes of the molecule which were found to have a temperature of 65 K. The authors of ref 11 suggested that their data were consistent with a torsional temperature of 300 K. Our precise combination differences and microwave-infrared double-resonance measurements definitively establish that the 974.9 and 974.3 cm^{-1} components of the spectrum both originate from the vibrational ground state and not from a torsional hot band. This assignment obviates the need for such a warm torsional vibration in the supersonic expansion of ref 11 and also is consistent with previous experiments by several of us where we have observed a degree of torsional cooling similar to that experienced by the other vibrational modes.[36]

It is interesting to speculate on the origin of the A″-symmetry perturbing state interacting with the assumed ν_{15} normal mode at 975 cm^{-1}. Our ability to identify the perturbing state requires reliable assignments and accurate frequencies for all the normal-mode vibrations below 975 cm^{-1}. Several conflicting normal-mode assignments have been proposed for HFC 134a. The results from these assignments for the normal modes are summarized in Table 8. Only modes with energies below 975 cm^{-1} need be considered. A possible perturbing state, selected on the basis of energy match to the ν_{15} level and the requirement of the same irreducible representation, that is A″ symmetry, is a combination vibration consisting of three quanta in the torsion and one quanta in the 666 cm^{-1} CF_3 symmetric deformation mode. If we choose (somewhat arbitrarily) the features in the spectral region of the torsion at 104.963 cm^{-1} as the $v = 1 \leftarrow 0$ torsional transition, at 102.95 cm^{-1} as the $v = 2 \leftarrow 1$ transition, and at 101.375 cm^{-1} as the $v = 3 \leftarrow 2$ transition, then $3\nu_{18} + \nu_8$ (where the ν_8 origin is chosen as 665.5 cm^{-1}, see Figure 5) is equal to 974.788 cm^{-1}, quite close to the observed high-resolution band positions. These choices for the torsional levels can be compared to the results of Raman measurements where the same level separations were given as 107, 106, and 102 cm^{-1}.[8] Of course it may be possible to choose a different set of torsional features that will also fit the requirements, and without detailed assignments for the torsional fine structure shown in Figure 5 we cannot be certain that these assignments are correct, but they are plausible. A $v = 1 \leftarrow 0$ torsional frequency of 104.9 cm^{-1} corresponds to a barrier of 13.7 kJ/mol ($V_3 = 1144$ cm^{-1}). This barrier gives values for the $v = 2 \leftarrow 1$ and $3 \leftarrow 2$ transitions of 102.3 and 99.5 cm^{-1} compared to the assigned values of 102.95 and 101.38 cm^{-1}. The discrepancies between these values could be compensated by the use of higher order terms in the Fourier expansion of the potential; however, the present uncertainty in the torsional analysis does not warrant such a detailed treatment.

A second reason for choosing the $3\nu_{18} + \nu_8$ assignment for the perturbing combination band is based upon observations[36] concerning torsional vibrations in HFC 143a, CF_3CH_3. In this molecule high-resolution infrared spectroscopy has demonstrated an anharmonic interaction between the ν_{10} fundamental near 970 cm^{-1} and the $2\nu_6 + \nu_{11}$ combination band. Here the ν_6 mode is the torsion, the ν_{11} mode is a CF_3 deformation, and the 970 cm^{-1} fundamental is the CH_3 rock. That assignment was confirmed by the observation of tunneling splittings in individual rovibrational transitions of the 970 cm^{-1} band due to internal rotation of the CH_3 group. This situation is similar to what we

propose for HFC 134a and gives us additional confidence that our identification of the general nature of the perturbing state as involving the torsion is correct, although as pointed out above any tunneling splitting in the spectrum of the HFC 134a molecule is below our experimental spectral resolution, which is not unexpected on the basis of the mass of the internal rotor and the conformational barrier height of ∼15 kJ/mol.[8]

We expect that the results of this study will be important for several reasons. First, it is likely that with increased use of hydrofluorocarbons such as HFC 134a their atmospheric concentration will increase in the future. It is presently believed that the primary route of removal of HFC 134a from the troposphere is via degradation to trifluoroacetyl fluorides followed by hydrolysis to trifluoroacetic acid.[37] The trifluoroacetic acid may be removed by precipitation in rainfall, and recently evidence has been presented for the appearance of elevated trifluoroacetic acid levels in seasonal wetlands.[38] Clearly atmospheric monitoring of HFC 134a (and trifluoroacetic acid) concentrations by infrared spectroscopy will be a valuable measure of these processes, and the assignment of HFC 134a vibrational modes and intensities is a prerequisite to such studies.[39] Second, several of us have recently presented results of vibrational studies of HFC 134a molecules adsorbed on the surface of NaX zeolite[10,40] that were undertaken in order to understand the ability of this zeolite to separate HFC 134a from its isomer HFC 134 (CF_2HCF_2H). Detailed modeling of the vibrational properties of the adsorbed species requires a good understanding of the molecular force field for the free molecule as a starting point, and it was for this reason that this study was begun. The measurements reported herein will thus also serve to facilitate interpretation of adsorbate spectra in catalytic systems. In fact, it is possible that HFC 134a may undergo heterogeneous atmospheric chemistry, for example on the surfaces of ice particles,[39] in addition to the homogeneous reactions already described, and perhaps increased understanding of surface chemical reactions will suggest interesting directions for atmospheric studies. Furthermore, from the purely spectroscopic perspective, understanding the vibrational spectrum of a molecule as "simple" as HFC 134a offers a test of our abilities to both experimentally resolve and theoretically describe a number of subtle intramolecular interactions, and the work presented here should stimulate further spectroscopic work on the fluorinated ethanes. In particular, high resolution far-infrared studies (see, for example, ref 41) of the internal rotations of fluorinated ethanes in molecular beams would be of great interest in furthering our understanding of the torsional potential energy surfaces for C−C bonds. Finally, we believe that we have demonstrated that thermodynamic properties (such as the ideal gas heat capacity) determined from either our vibrational data or the results of *ab initio* calculations are now sufficiently accurate for use in equation-of-state treatments of thermodynamic properties for HFC 134a.

Acknowledgment. The authors would like to thank David Corbin (DuPont) for furnishing the sample of HFC 134a used in the present investigation and W. Lafferty (NIST) for helpful discussions. Partial support from the NASA Upper Atmosphere Research Program (UARP) is also acknowledged.

References and Notes

(1) Chen, S. S.; Rodgets, A. S.; Chao, J.; Wilhoit, R. C.; Zwolinski, B. J. *J. Phys. Chem. Ref. Data* **1975**, *4*, 441.
(2) Ogata, T.; Miki, Y. *J. Mol. Struct.* **1986**, *140*, 49.
(3) Danti A.; Wood, J. L. *J. Chem. Phys.* **1959**, *30*, 582.
(4) Edgell, W. F.; Riethof, T. R.; Ward, C. *J. Mol. Spectrosc.* **1963**, *11*, 92.
(5) Nielsen, J. R.; Halley, C. J. *J. Mol. Spectrosc.* **1965**, *17*, 341.
(6) Harnish, D. F.; Hirschmann, R. P. *Appl. Spectrosc.* **1970**, *24*, 28.
(7) Papasavva, S.; Tai, S.; Esslinger, A.; Illinger, K. H.; Kenny, J. E. *J. Phys. Chem.* **1995**, *99*, 3438.
(8) Lopata, A. D.; Durig, J. R. *J. Raman Spectrosc.* **1977**, *6*, 61.
(9) Cappellani, F.; Restelli, G. *Spectrochim. Acta* **1992**, *48A*, 1127.
(10) Crawford, M. K.; Corbin, D. R.; Smalley, R. J. In *Amazing Light: A Festschrift in Honor of Charles Hard Townes on His 80th Birthday*; Chaio, R. Y., Ed.; Springer-Verlag: Berlin, 1996.
(11) McNaughton, D.; Evans, C.; Robertson, E. G. *J. Chem. Soc., Faraday Trans.* **1995**, *91*, 1723.
(12) Crowder, G. A. *J. Fluorine Chem.* **1973/74**, *3*, 125.
(13) Lucas, K.; Delfs, U.; Buss, V.; Speis, M. *Int. J. Thermophys.* **1993**, *14*, 993.
(14) Balle, T. J; Flygare, W. H. *Rev. Sci. Instrum.* **1981**, *52*, 33.
(15) Lovas, F. J.; Suenram, R. D. *J. Chem. Phys.* **1987**, *87*, 2010. Lovas, F. J.; Suenram, R. D.; Fraser, G. T.; Gillies, C. W.; Zozom, J. *Ibid.* **1988**, *88*, 722.
(16) Lovas, F. J.; Zobov, N.; Fraser, G. T.; Suenram, R. D. *J. Mol. Spectrosc.* **1995**, *171*, 189.
(17) Grabow, J.-U.; Stahl, W. *Z. Naturforsch* **1990**, *45A*, 1043.
(18) Fraser, G. T.; Pine, A. S.; Kreiner, W. A. *J. Chem. Phys.* **1991**, *94*, 7061.
(19) Watson, J. K. G. in *Vibrational Spectra and Structure*; Durig, J. R., Ed.; Elsevier: Amsterdam, 1978; pp 1−89.
(20) Edgell, W. E.; Miller, G. H.; Amy, J. W. *J. Am. Chem. Soc.* **1957**, *79*, 2391.
(21) Beagley, B.; Jones, M. A.; Zanjanchi, M. A. *J. Mol. Struct.* **1979**, *56*, 215.
(22) Hayashi, M.; Fujitake, M.; Inagusa, T.; Miyazaki, S. *J. Mol. Struct.* **1990**, *216*, 9.
(23) Beagley, B.; Jones, M. O.; Yavari, P. *J. Mol. Struct.* **1981**, *71*, 203.
(24) Kraitchman, J. *Am. J. Phys.* **1953**, *21*, 17.
(25) See, for example: Herzberg, G. *Molecular Spectra and Molecular Structure II. Infrared and Raman Spectra of Polyatomic Molecules*; Van Nostrand Reinhold: New York, 1945; Chapters 5 and 6. Allen, H. C.; Cross, P. C. *Molecular Vib-Rotors*; Wiley: New York, 1963.
(26) Overend, J. In *Studies in Physical and Theoretical Chemistry 20: Vibrational Intensities in Infrared and Raman Spectroscopy*; Person, W. B., Zerbi, G., Eds.; Elsevier: New York, 1982; Chapter 2.
(27) van der Veken, B. J. in *Vibrational Spectra and Structure*; Durig, J. R., Ed.; Elsevier: New York, 1986; Vol. 15, Chapter 6.
(28) Frisch, M. J.; Trucks, G. W.; Schlegel, H. B.; Gill, P. M. W.; Johnson, B. G.; Robb, M. A.; Cheeseman, J. R.; Keith, T.; Petersson, G. A.; Montgomery, J. A.; Raghavachari, K.; Al-Laham, M. A.; Zakrzewski, V. G.; Ortiz, J. V.; Foresman, J. B.; Cioslowski, J.; Stefanov, B. B.; Nanayakkara, A.; Challacombe, M.; Peng, C. Y.; Ayala, P. Y.; Chen, W.; Wong, M. M.; Andres, J. L.; Replogle, E. S.; Gomperts, R.; Martin, R. L.; Fox, D. J.; Binkley, J. S.; Defrees, D. J.; Baker, J.; Stewart, J. P.; Head-Gordon, M.; Gonzalez, C.; Pople, J. A. *Gaussian 94*; Gaussian, Inc.: Pittsburgh, 1995.
(29) Pople, J. A.; Schlegel, H. B.; Krishnan, R.; Defrees, D. J.; Binkley, J. S.; Frisch, M. J.; Whiteside, R. A.; Hout, R. F.; Hehre, W. J. *Int. J. Quant. Chem. Symp.* **1981**, *15*, 269; Pople, J. A.; Scott, A. P.; Wong, M. W.; Radom, L. *Isr. J. Chem.* **1993**, *33*, 345.
(30) Meyer, C. W.; Morrison, G. *J. Phys. Chem.* **1991**, *95*, 3860.
(31) Wilson, E. B. *Chem. Rev.* **1940**, *27*, 17. Aston, J. G. In *A Treatise on Physical Chemistry*; Van Nostrand: New York, 1942; Vol. 1, Chapter 4. Godnev, I. N. *Calculation of Thermodynamic Functions from Molecular Data*; U.S. Atomic Energy Commission, AEC-tr-3855, 1956.
(32) Ward, C. R.; Ward, C. H. *J. Mol. Spectrosc.* **1964**, *12*, 289.
(33) Tillner-Roth, R.; Baehr, H. D. *J. Phys. Chem. Ref. Data* **1994**, *23*, 657.
(34) Lisal, M.; Vacek, V. *Mol. Phys.* **1996**, *87*, 167.
(35) Chen, Y.; Paddison, S. J.; Tschuikow-Roux, E. *J. Phys. Chem.* **1994**, *98*, 1100.
(36) Fraser, G. T.; Pine, A. S.; Domenech, J. L.; Pate, B. H. *J. Chem. Phys.* **1993**, *99*, 2396.
(37) Wallington, T. J.; Hurley, M. D.; Ball, J. C.; Kaiser, E. W. *Environ. Sci. Technol.* **1992**, *26*, 1318.
(38) Tromp, T. K.; Ko, M. K. W.; Rodriguez, J. M.; Sze, N. D. *Nature* **1995**, *376*, 327.
(39) Goody, R. *Principles of Atmospheric Physics and Chemistry*; Oxford: New York, 1995.
(40) Udovic, T. J.; Nicol, J. M.; Cavanagh, R. R.; Rush, J. J.; Crawford, M. K.; Grey, C. P.; Corbin, D. R. *Mater. Res. Soc. Symp. Proc.* **1995**, *376*, 751.
(41) Cruzan, J. D.; Braly, L. B.; Liu, K.; Brown, M. G.; Loeser, J. G.; Saykally, R. J. *Science* **1996**, *271*, 59.